LUNAR GEOLOGY

Isotopic and compositional constraints on the source of basalt collected from the lunar farside

Xiaochao Che[1,2]*, Tao Long[1,2]*, Alexander Nemchin[1,3], Shiwen Xie[1,2], Le Qiao[4], Zengsheng Li[5], Yiyi Ban[1], Runlong Fan[1,2], Chun Yang[1], Dunyi Liu[1,5]

Volcanism on the Moon has produced surface basalt deposits, which record lunar interior processes. The Chang'e-6 mission retrieved samples from the South Pole–Aitken basin (SPA) on the Moon's far side. We analyzed basalt fragments collected by Chang'e-6 and found that their composition resembles that of low-titanium basalts previously sampled by the Apollo missions. Uranium-lead (U-Pb) dating indicated a basalt age of 2823.0 ± 5.9 million years and a source $^{238}U/^{204}Pb$ ratio (μ-value) of 480 ± 56. This high μ-value indicates that the source contained materials that formed during the late stages of lunar magma ocean (LMO) crystallization. The results are consistent with the LMO model, but the Chang'e-6 basalt deviates from the trend in Apollo mission samples of younger basalts having higher μ-values. We suggest that this indicates post-LMO modification of the mantle by the SPA impact.

The Apollo, Luna, and Chang'e-5 sample-return missions obtained samples from multiple locations on the Moon's near side, informing our understanding of lunar evolution and the development of the lunar magma ocean (LMO) model (*1*). In this model, the lunar mantle was initially stratified by magma ocean crystallization and then subsequently experienced gravitational overturn, when denser layers that had accumulated on top of the magma sank to the bottom. The LMO model explains lunar crust formation and predicts a reservoir enriched in incompatible elements (those that concentrate in the melt rather than in solid minerals). This reservoir is known as KREEP, owing to its high concentrations of potassium (K), rare earth elements (REE), and phosphorus (P) (*1*–*4*). The LMO model underpins our understanding of the Moon's later magmatic history, including volcanism that produced basaltic rocks recovered by sample-return missions.

The limitation of previous sample collection to the near side of the Moon may have biased our understanding of lunar history, owing to incomplete coverage of the range of rock types present on the Moon. Near and far side differences are evident in remote-sensing observations (*5*), including investigations of lunar gravity, topography, and surface composition (*6*). It remains uncertain whether the LMO was global or restricted to the near side of the Moon (*7*, *8*). Surface exposures of KREEP-rich material are restricted to the Procellarum KREEP terrane on the near side of the Moon (*9*), which might reflect limited KREEP distribution in the underlying mantle. Investigation of these issues requires samples from the far side of the Moon.

The Chang'e-6 spacecraft landed within the South Pole–Aitken (SPA) basin on the far side, a region predicted to have a chemical makeup and geology distinct from all nearside landing sites (see supplementary text). Half of the rock fragments present in the samples are basalts. We investigated 33 of these basaltic fragments from a Chang'e-6 soil subsample. Previous studies (*10*, *11*) of similar fragments found that the basalt source is KREEP-free, suggesting that the KREEP reservoir may be a localized feature of the near side of the Moon or possibly that the LMO was not a global phenomenon. We explored these issues using U-Pb dating and Pb isotope systematics of Chang'e-6 basalts.

Textures and composition of the fragments

All the investigated fragments are rich in the minerals common in basalts, such as plagioclase [a mixture of albite (Ab-$NaAlSi_3O_8$) and anorthite (An-$CaAl_2Si_2O_8$)] and pyroxene [a mixture of wollastonite (Wo-$Ca_2Si_2O_6$), enstatite (En-$Mg_2Si_2O_6$), and ferrosilite (Fs-$Fe_2Si_2O_6$)], with subordinate ilmenite. These minerals define textures observed in the fragments that range from porphyritic [larger grains surrounded by smaller ones (Fig. 1A)] to subophitic (plagioclase partially enclosed by pyroxene), and poikilitic (smaller plagioclase grains scattered within larger pyroxene grains) (Fig. 1, B and C). Several fragments are dominated by mesostasis (interstitial material between the grains), which represents the last-crystallized melt (Fig. 1D). Some fragments contain minor olivine [a mixture of forsterite (Fo-Mg_2SiO_4) and fayalite (Fa-Fe_2SiO_4)], Cr-spinel, K-feldspar, troilite, K-glass, and silica (data S1 and S2). Many also contain accessory apatite, baddeleyite, and zirconolite, ranging in size from a few microns to a few tens of microns. Mineral compositions vary systematically with texture (Fig. 2, A and B) (see supplementary text), which indicates crystallization from a single basaltic melt. They also align with the trends identified in low-Ti basalts collected by the Apollo missions (Fig. 2, A and B) (*12*).

The Chang'e-6 basalts are coarse grained (data S1). Consequently, bulk compositions reconstructed from images of fragments about 500 microns in size and electron microprobe (EMP) data (table S1) might not be representative of the composition of the parent rocks. We therefore calculated the average compositions for fragments representing different textural types and the overall average for all fragments, which we compared with each other and to the existing classification scheme for mare (lunar plain) basalts (*13*, *14*).

The abundances of major rock-forming elements in the fragments vary systematically from porphyritic, through subophitic and poikilitic, to mesostasis-rich fragments. We found a decreasing trend for MgO (8.7, 4.3, and 0.4% in those three groups, respectively), with a corresponding decline in other oxides except FeO. This is consistent with crystallization of plagioclase and progressively more Fe-rich pyroxene. TiO_2 concentrations are highest in subophitic to poikilitic fragments (6.6%) compared with porphyritic (4.8%) and mesostasis-rich (5.5%) fragments, possibly indicating delayed ilmenite formation. The overall average composition (table S1) has 5.5% TiO_2, 11.3% Al_2O_3, and 0.08% K_2O. This classifies the Chang'e-6 basalt as a low-Ti and low-K basalt, though it is on the borderline between low- and high-Al groups (*13*).

The concentrations of REE determined in selected pyroxene grains (data S3) change systematically with the MgO content (Fig. 2C). The Mg-rich parts of the pyroxene grains [Mg/(Mg+Fe) between 0.20 and 0.65] show little, if any, change in REE concentrations, but pyroxenes with Mg/(Mg+Fe) <0.2 display a rapid increase in REE contents (Fig. 2C), consistent with fractional crystallization. We used the near-constant REE concentrations in pyroxene with Mg/(Mg+Fe) >0.2 to estimate the REE concentrations in the melt that coexisted with this pyroxene. The resulting REE pattern [normalized to carbonaceous chondrite meteorites (*15*)] (Fig. 2D) is convex, with a moderate Eu anomaly [$Eu_N/(Sm_N \times Gd_N)^{0.5}$, where subscript N indicates chondrite normalized values] and about 20 times the REE abundance of chondrites. This enrichment in REEs in the Chang'e-6 basalt melt, and the overall REE pattern, matches those in low-Ti basalts collected by the Apollo missions (Fig. 2D) (*16*).

U-Pb isotopic analysis

To determine the age of the Chang'e-6 fragments, we used an ion microprobe to measure Pb isotopes for selected apatite grains, Zr-rich minerals (zirconolite and baddeleyite), and

[1]Beijing Sensitive High Resolution Ion Micro Probe Center, Institute of Geology, Chinese Academy of Geological Sciences, Beijing, China. [2]Tiandu Deep Space Exploration Joint Laboratory, Institute of Geology, Chinese Academy of Geological Sciences, Beijing, China. [3]School of Earth and Planetary Sciences, Curtin University, Perth, WA, Australia. [4]Shandong Key Laboratory of Optical Astronomy and Solar-Terrestrial Environment, School of Space Science and Technology, Institute of Space Sciences, Shandong University, Weihai, China. [5]Shandong Institute of Geological Sciences, Jinan, China.
*Corresponding author. Email: cxc@bjshrimp.cn (X.C.); longtao@bjshrimp.cn (T.L.)

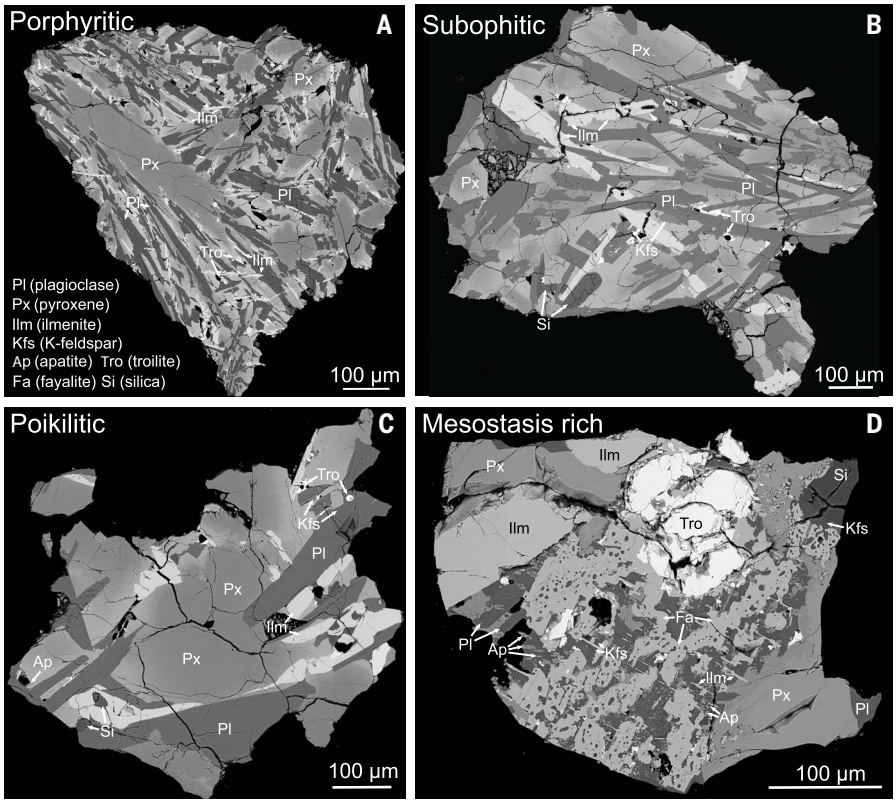


Fig. 1. Typical basaltic fragments from the Chang'e-6 sample, illustrating different textures. Backscattered electron images of (**A**) porphyritic, (**B**) subophitic, (**C**) poikilitic, and (**D**) mesostasis-rich fragments. Labels indicate abbreviated mineral names; see legend in (A).

feldspars (table S2). For apatite, we also analyzed U isotopes to provide an additional check on the derived ages and detect any events that may have reset the U-Pb isotope system. Most (18 out of 23) analyses of 19 apatite grains follow a short trend on a Pb isotope plot (Fig. 3A), pointing toward terrestrial Pb composition, which indicates a small level of terrestrial Pb contamination. Another five analyses follow a steeper trend, indicating the presence of initial lunar Pb (Fig. 3A). U-Pb ages of three separate fragments determined from multiple analyses of apatite grains (table S2) are indistinguishable within their uncertainties (fig. S2, A to C), so we concluded that all fragments represent the same basaltic unit, which is also supported by their mineralogy and bulk composition (see supplementary text). We therefore combined the data for different fragments to define a single (more precise) age of this unit. Figure 3C shows contamination-corrected data for 18 analyses of the U-Pb isotope system, which indicate an age of 2843 ± 33 million years (Ma).

No suitable U-Pb isotopic standard exists for zirconolite, so all Zr-rich grains were analyzed for Pb isotopes only. Figure S2, D to F, shows $^{207}Pb/^{206}Pb$ and $^{204}Pb/^{206}Pb$ ratios measured for multiple apatite and Zr-rich grains taken from three fragments. We again found consistent ages, so we combined all fragments to determine an average age of 2823.0 ± 5.9 Ma (Fig. 3B). This is consistent with the U-Pb age of apatite but is more precise; we therefore adopted it as our preferred estimate for the age of the Chang'e-6 basalt.

Sixteen K-feldspar grains were analyzed to assess the initial Pb composition of the basalt. Figure 3B shows that these analyses follow a steep trend on a $^{207}Pb/^{206}Pb$ versus $^{204}Pb/^{206}Pb$ isotope ratio plot, along with five apatite analyses. We interpret this as being due to varying mixtures of Pb formed in situ, from radioactive decay of U, with initial Pb. We attribute the scatter in this plot to terrestrial contamination in some analyses. A group of six analyses with the highest $^{207}Pb/^{206}Pb$ ratios follow a trend toward terrestrial Pb composition (Fig. 3B), which we attribute to binary mixing between initial Pb and terrestrial Pb contamination. We adopted the two analyses with the lowest $^{204}Pb/^{206}Pb$ ratios as an estimate of the initial Pb composition of the basalt and found $^{204}Pb/^{206}Pb = 0.00439 \pm 0.00047$, $^{207}Pb/^{206}Pb = 1.059 \pm 0.010$, and $^{208}Pb/^{206}Pb = 0.909 \pm 0.013$.

We combined this initial Pb composition with the measured age to estimate the initial $^{238}U/^{204}Pb$ ratio (μ-value) of the basalt's mantle source. This calculation assumes a two-stage model evolution, in which the LMO forms at time T_0 with a μ-value of μ_0, followed by crystallization of the basalt source at time T_s with μ_s (*12*). We followed previous methods to estimate μ_s (*17*) and found that the Chang'e-6 basalt source had a μ-value of 480 ± 56. This value is higher than those found in previous studies (*10*, *11*). We ascribe this discrepancy to our adoption of a different model (*17*) and the assumed fixed values of μ_0 and T_0 in the previous work (we allowed both to vary in our model fitting).

KREEP mixing in lunar basalts

Lunar mare and KREEP basalts are thought to be indirectly linked to the crystallization of LMO, which initially formed a stratified mantle with different layers composed of different mineral assemblages (*1*, *3*). Subsequent gravitational mantle overturn (*2*) mixed these layers but did not completely erase their differences, producing distinct sources for the formation of compositionally diverse basaltic melts. The KREEP reservoir (*18*) formed from the last remnants of the highly differentiated LMO melt, enriched in incompatible elements. High concentrations of these elements in some mare basalt samples, and/or isotopic evidence of such enrichment in their source, have been interpreted as indicating that KREEP-rich materials were incorporated into the basaltic melts (*19*–*21*). This addition could occur through mechanisms ranging from mantle mixing (before melt formation) to the assimilation of KREEP during the magma's ascent to the surface or while on the surface (*22*, *23*). Pb isotope systematics of many samples have also been interpreted as being due to the addition of KREEP to mare basalt melts (*23*–*25*). However, enrichment of incompatible elements in some basalts could be also produced by fractionation of basaltic melts or low degrees of mantle melting during their formation (*26*, *27*). Therefore, chemically similar compositions of different lunar basalts may form with or without KREEP involvement.

We applied this reasoning to the Chang'e-6 fragments. The REE abundances in pyroxene grains vary by an order of magnitude (Fig. 2C), which could indicate a KREEP contribution. However, assimilation of KREEP by crystallizing melt would preferentially increase light REE abundances in pyroxene and plagioclase as crystallization progresses (*26*). The chondrite-normalized La/Yb ratio in pyroxenes from Chang'e-6 fragments ranges from 0.02 to 0.24 but does not vary systematically with their Mg content. Similarly, the slope of the REE patterns that we measured for plagioclase grains (Fig. 2E) does not change with their anorthite contents. Both observations indicate that there was no KREEP assimilation by the basalt melt during crystallization. Similarly, the flat REE pattern and low REE abundances that we calculated for the Chang'e-6 basalt melt composition (Fig. 2D) are not consistent with the addition of KREEP material to the melt or its mantle source before onset of crystallization.

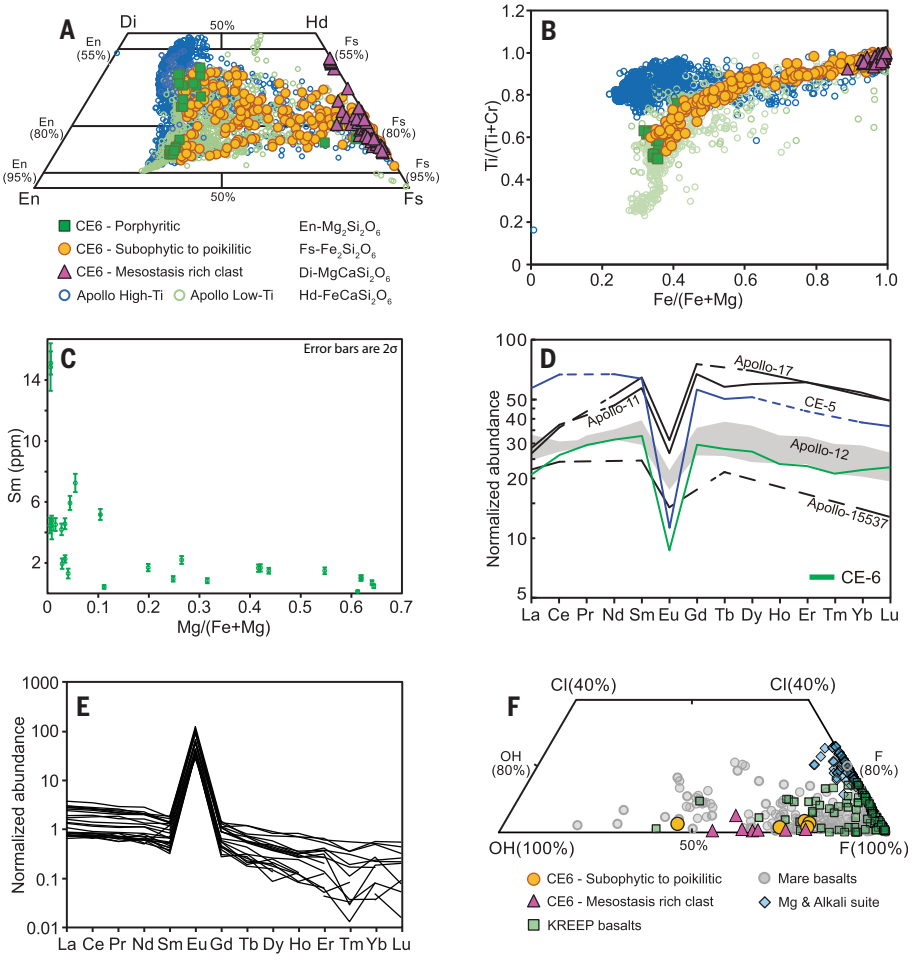


Fig. 2. Mineral chemistry of the Chang'e-6 basaltic fragments. (**A**) Compositions of pyroxene in the fragments. High- and low-Ti samples from the Apollo missions are plotted for comparison (*12*). (**B**) Fe/(Fe + Mg) as a function of Ti/(Ti + Cr) measured in pyroxene (*12*). Abbreviations are the same as in (A). (**C**) Sm abundance as a function of Mg/(Fe + Mg) measured in pyroxene. ppm, parts per million. (**D**) REE abundance pattern of Chang'e-6 basalt source (CE-6), normalized to chrondritic meteorites (*15*). Patterns for Chang'e-5 (CE-5) (*27*) and Apollo mission basalt sources (*16*) are shown for comparison. The gray shading indicates the range spanned by several Apollo 12 samples. Values are provided in data S3. Dashed sections of lines indicate no data provided in the original publication. (**E**) REE abundance patterns measured for plagioclase in the Chang'e-6 fragments. (**F**) Proportions of F-Cl-OH abundances in apatite from the Chang'e-6 basalt. Mare and KREEP basalts as well as Mg and Alkali suites (*42*) are shown for comparison.

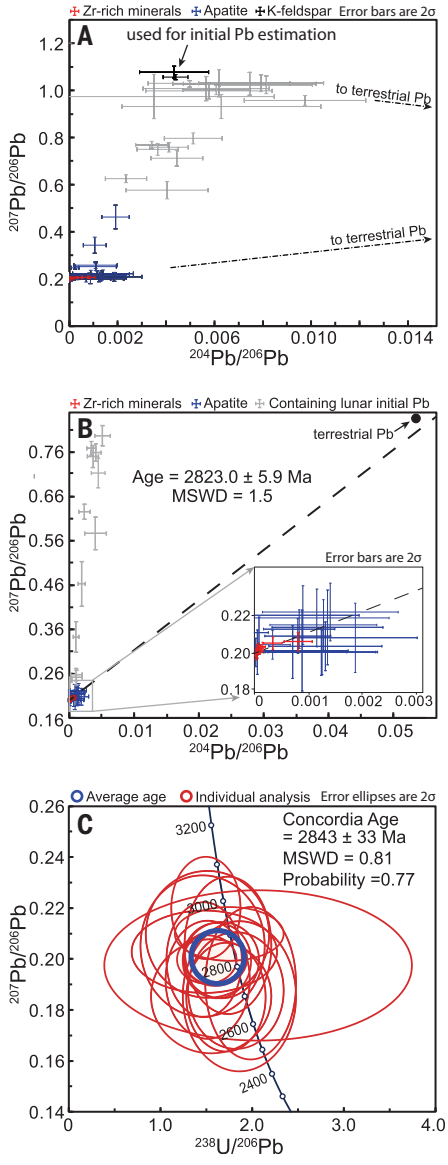


Fig. 3. U-Pb and Pb-Pb isotope data measured for Chang'e-6 basalt. (**A**) The isotope ratio $^{207}Pb/^{206}Pb$ as a function of $^{204}Pb/^{206}Pb$ for different minerals. (**B**) The same ratios as in (A) measured for Zr-rich minerals (red crosses) and apatite (blue crosses). Gray crosses represent data that contain lunar initial Pb, which were excluded from the age calculation. The dashed line is the isochron model fitted to the remaining data. MSWD, mean squared weighted deviation. (**C**) $^{207}Pb/^{206}Pb$ versus $^{238}U/^{206}Pb$ diagram, showing apatite U-Pb data. The curve indicates the expected $^{207}Pb/^{206}Pb$ and $^{238}U/^{206}Pb$ values for the labeled ages (in Ma).

For several lunar meteorites, the proportions of volatile species (Cl, F, OH) in apatite indicate no KREEP addition to those basalts (*26*). We found a similar result for Chang'e-6 basalt: Volatiles in the apatite grains that we investigated are dominated by F and OH, with little to no Cl (Fig. 2F). This is unlike apatite from KREEP-rich rocks, which are enriched in Cl (*26*). This reasoning leads to the conclusion that the composition of the Chang'e-6 basalt fragments indicates no KREEP contribution.

Previous conclusions of no KREEP contribution to other lunar basalt samples were supported by Sr and Nd isotopic data (*26*–*29*). Similar arguments have been applied in previous studies of the Chang'e-6 basalt, which independently concluded that there was no KREEP addition to their melt or source (*10*, *11*).

Pb isotope evidence of KREEP contribution

Comparing samples from multiple missions and meteorites, the μ-values for the sources of low-Ti lunar basalts span an order of magnitude (Fig. 4D). If the sources of all these basalts are linked to different mineral assemblages successively accumulated during LMO crystallization, the observed range of μ-values is hard to explain without KREEP addition to most of these sources. U and Pb are among the most incompatible elements, so we expect that the ratio of these elements (and therefore the μ-value) did not change substantially in the LMO melt as crystallization progressed. Consequently, mineral assemblages formed at different stages of crystallization should have μ-values controlled only by the mineral-melt partition coefficients. Therefore, differences in μ-values between mineral assemblages formed during LMO crystallization should not reach the order-of-magnitude range observed in lunar basalt sources (Fig. 4D), as the relative partitioning of U and Pb into major lunar mantle constituents, such as olivine, orthopyroxene, and clinopyroxene, is similar (*30*–*32*). More extensive data are available for terrestrial rocks, indicating

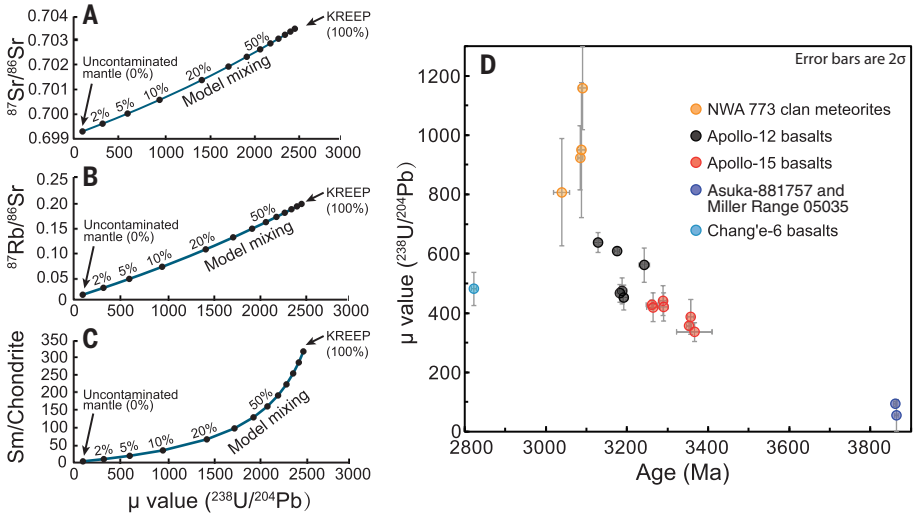


Fig. 4. Isotopic and abundance characteristics of Chang'e-6 basalt. Model mixing relationships between lunar mantle and KREEP (*12*), each plotted as a function of μ-value; labels indicate the KREEP contribution. (**A**) Initial $^{87}Sr/^{86}Sr$. (**B**) $^{87}Rb/^{86}Sr$. (**C**) Sm abundance, normalized to the chondritic value. (**D**) Relationships between the crystallization ages and μ-values of the magma sources for low-Ti lunar basalts. Our results for Chang'e-6 are compared with those for Apollo mission basalts (*25*), NWA 773 clan meteorites (*40*), and Yamato-793169 and Asuka-881757 meteorites (*17*).

that high-μ terrestrial reservoirs with values of 20 to 50 are linked to processes enabled by plate tectonics (*33*, *34*), which does not occur on the Moon. We concluded that the processes of melting and fractional crystallization of common rock-forming minerals alone cannot produce μ-values that span an order of magnitude.

To explain the range of μ-values in lunar basalts within the LMO model, we considered an initially high μ-value of the LMO melt (or bulk silicate Moon), which was likely due to volatile loss during the Moon's formation (*35*). The high μ-value of the melt persists during crystallization as a result of the strongly incompatible nature of both U and Pb, until the final remnants of this melt formed the KREEP reservoir. Mineral assemblages formed at different stages of crystallization would then have lower μ-values than the coexisting melt, but this process alone cannot produce the observed range of μ-values. Instead, achieving this order-of-magnitude variation requires the mixing of KREEP materials into the mare basalt magmas during their assent or into their sources before melting (*17*).

This raises a contradiction between (i) the Pb isotope systematics, which indicate the addition of KREEP, and (ii) insights from other isotope systems (e.g., Rb-Sr and Sm-Nd) and compositional data for many lunar basalts, which indicate no KREEP content. However, the U-Pb isotopic system is more sensitive to small additions of KREEP material than either the Rb-Sr or Sm-Nd systems because Pb was depleted on the Moon during its formation (*35*). The Pb abundances in various lunar rocks and reservoirs are therefore determined by accumulation of radiogenic Pb, formed from U decay. As a result of this, and the greater incompatibility of both U and Pb compared with Sr and Nd, the contrast between Pb concentrations in KREEP-rich and KREEP-free materials is stronger than that of Sr and Nd (*36*). The difference in concentration contrasts leads to nonlinear mixture models (*12*) (Fig. 4, A to C). These models demonstrate that low proportions of KREEP mixing cause Pb isotopes and μ-values to vary more strongly than the Sr isotope compositions (Fig. 4A). An increase in μ-value from 100 to 500 is equivalent to a change in $^{87}Sr/^{86}Sr$ of about 0.1%, which is often difficult to detect. The same conclusion applies to mixtures of materials from reservoirs with differing $^{87}Rb/^{86}Sr$ ratios (Fig. 4B). For the abundances of REEs, this effect is even more pronounced; using Sm as an example, the same change of μ-value corresponds to a change in Sm abundance from about three times that of chondritic meteorites [assumed to represent lunar mantle materials (*37*)] to about 20 times the chondritic value (Fig. 4C). That is roughly the level of REE enrichment we estimated for the Chang'e-6 melt (Fig. 2D).

Comparison with other lunar basalt samples

We found a disparity between the composition of the Chang'e-6 basalt, which does not indicate KREEP involvement in its formation, and the Pb isotope data, which indicate addition of 3 to 4% of KREEP (Fig. 4, A to C). This disparity is also evident in some lunar meteorites, such as NWA 4734, and the Chang'e-5 basalt, which have source μ-values of about 1200 and 700, respectively (*38*–*40*). All these basalts require addition of KREEP, either by mixing before the melting of the sources or assimilation after melt formation (but before crystallization) to explain their high μ-values.

Alternatively, other processes after LMO crystallization might have produced sources with high U/Pb at specific locations on the Moon. For example, the SPA impact might have melted the underlying mantle, causing volatile loss and depletion in Pb. This possibility is supported by the observed relationships between the ages and source μ-values of lunar low-Ti basalts (Fig. 4D). All low-Ti basalt samples for which Pb isotope systems have been studied display a trend of higher μ-values at younger ages, which the Chang'e-6 basalt does not follow (Fig. 4D). It has been suggested that this trend could indicate a gradual increase in mixing of KREEP material into the mantle, owing to erosion of the KREEP layer located under the lunar crust by mantle convection for 1 billion or 2 billion years after LMO crystallization (*17*).

The discrepancy between the Chang'e-6 sample and other lunar basalts could arise if different regions of the Moon (such as the Procellarum KREEP terrane, SPA region, and areas dominated by plagioclase rich crust) evolved differently after LMO crystallization. One of these differences could be variable modification of different regions of lunar mantle by basin-forming impacts, such as the SPA. This is consistent with a previous proposal that some moderately volatile elements in Apollo samples were affected by basin-forming impacts (*41*). This would not invalidate the LMO model but implies a more complex history, involving initial differentiation and stratification of the lunar mantle during LMO crystallization followed by mantle overturn and further transformation of upper parts of the mantle by basin-forming events. Such a transformation could also provide the conditions required to trigger later phases of basaltic magmatism.

REFERENCES AND NOTES

1. P. H. Warren, *Annu. Rev. Earth Planet. Sci.* **13**, 201–240 (1985).
2. P. C. Hess, E. M. Parmentier, *Earth Planet. Sci. Lett.* **134**, 501–514 (1995).
3. A. M. Gaffney *et al.*, *Rev. Mineral. Geochem.* **89**, 103–145 (2023).
4. L. T. Elkins-Tanton, S. Burgess, Q.-Z. Yin, *Earth Planet. Sci. Lett.* **304**, 326–336 (2011).
5. G. H. Heiken, D. T. Vaniman, B. M. French, *Lunar Sourcebook, A User's Guide to the Moon* (Cambridge Univ. Press, 1991).
6. B. L. Jolliff, J. J. Gillis, L. A. Haskin, R. L. Korotev, M. A. Wieczorek, *J. Geophys. Res.* **105**, 4197–4216 (2000).
7. L. E. Borg, J. N. Connelly, M. Boyet, R. W. Carlson, *Nature* **477**, 70–72 (2011).
8. L. E. Borg *et al.*, *Earth Planet. Sci. Lett.* **523**, 115706 (2019).
9. J. J. Gillis, B. L. Jolliff, R. L. Korotev, *Geochim. Cosmochim. Acta* **68**, 3791–3805 (2004).
10. Q. W. L. Zhang *et al.*, *Nature* 10.1038/s41586-024-08382-0 (2024).
11. Z. Cui *et al.*, *Science* **386**, 1395–1399 (2024).
12. Materials and methods are available as supplementary materials.
13. C. R. Neal, L. A. Taylor, *Geochim. Cosmochim. Acta* **56**, 2177–2211 (1992).
14. C. K. Shearer *et al.*, *Rev. Mineral. Geochem.* **60**, 365–518 (2006).
15. E. Anders, N. Grevesse, *Geochim. Cosmochim. Acta* **53**, 197–214 (1989).
16. L. J. Hallis, M. Anand, S. Strekopytov, *Geochim. Cosmochim. Acta* **134**, 289–316 (2014).
17. R. E. Merle, A. A. Nemchin, M. J. Whitehouse, G. G. Kenny, J. F. Snape, *J. Petrol.* **65**, egae062 (2024).
18. P. H. Warren, J. T. Wasson, *Rev. Geophys.* **17**, 73–88 (1979).

19. L. E. Nyquist, B. M. Bansal, H. Wiesmann, in *Proceedings of the Sixth Lunar Science Conference* (Pergamon Press, 1975), pp. 1445–1465.
20. R. Carlson, G. Lugmair, *Earth Planet. Sci. Lett.* **45**, 123–132 (1979).
21. L. E. Nyquist, C. Y. Shih, *Geochim. Cosmochim. Acta* **56**, 2213–2234 (1992).
22. B. L. Jolliff, R. L. Korotev, R. A. Zeigler, C. Floss, *Geochim. Cosmochim. Acta* **67**, 4857–4879 (2003).
23. Y. Wang *et al*., *Geochim. Cosmochim. Acta* **92**, 329–344 (2012).
24. J. F. Snape, B. Davids, A. A. Nemchin, M. J. Whitehouse, J. J. Bellucci, *Chem. Geol.* **482**, 101–112 (2018).
25. J. F. Snape *et al*., *Geochim. Cosmochim. Acta* **266**, 29–53 (2019).
26. S. M. Elardo *et al*., *Meteorit. Planet. Sci.* **49**, 261–291 (2014).
27. H.-C. Tian *et al*., *Nature* **600**, 59–63 (2021).
28. L. E. Borg *et al*., *Geochim. Cosmochim. Acta* **73**, 3963–3980 (2009).
29. Y. Srivastava, A. Basu Sarbadhikari, J. M. D. Day, A. Yamaguchi, A. Takenouchi, *Nat. Commun.* **13**, 7594 (2022).
30. I. N. Bindeman, A. M. Davis, *Geochim. Cosmochim. Acta* **64**, 2863–2878 (2000).
31. T. H. Green, *Chem. Geol.* **117**, 1–36 (1994).
32. I. N. Bindeman, A. M. Davis, M. J. Drake, *Geochim. Cosmochim. Acta* **62**, 1175–1193 (1998).
33. T. Hanyu *et al*., *Geochim. Cosmochim. Acta* **143**, 232–252 (2014).
34. J. C. Lassiter, J. Blichert-Toft, E. H. Hauri, H. G. Barsczus, *Chem. Geol.* **202**, 115–138 (2003).
35. R. M. Canup *et al*., *Rev. Mineral. Geochem.* **89**, 53–102 (2023).
36. J. F. Snape *et al*., *Geochim. Cosmochim. Acta* **326**, 119–148 (2022).
37. G. A. Snyder, L. A. Taylor, C. R. Neal, *Geochim. Cosmochim. Acta* **56**, 3809–3823 (1992).
38. Q.-L. Li *et al*., *Nature* **600**, 54–58 (2021).
39. X. Che *et al*., *Science* **374**, 887–890 (2021).
40. R. E. Merle *et al*., *Meteorit. Planet. Sci.* **55**, 1808–1832 (2020).
41. J. J. Barnes *et al*., *Earth Planet. Sci. Lett.* **447**, 84–94 (2016).
42. F. M. McCubbin *et al*., *Rev. Mineral. Geochem.* **89**, 729–786 (2023).
43. China National Space Administration, "Notice of China National Space Administration on the distribution of procedures for requesting lunar samples" [in Chinese and English] (2020); www.cnsa.gov.cn/n6758823/n6758839/c6811124/content.html.

ACKNOWLEDGMENTS

We thank the China National Space Administration (CNSA) for providing access to the lunar sample CE6C0010YJFMFM004. We appreciate thoughtful comments from J. Levine and two anonymous reviewers. We also thank R. Pidgeon for providing comments on the revised version of the manuscript. **Funding:** T.L., X.C., and D.L. were funded by The National Key Research and Development Program of China, from the Ministry of Science and Technology of the People's Republic of China, grant no. 2022YFF0704900. D.L., X.C., T.L., and A.N. were funded by the National Natural Science Foundation of China, grant nos. 42241107 and 42241158. **Author contributions:** X.C., A.N., T.L., and D.L. designed the project. X.C., T.L., A.N., S.X., C.Y., Z.L., L.Q., Y.B., and R.F. collected analytical data. X.C., T.L., A.N., and S.X. produced tables and figures and performed calculations. X.C., A.N., T.L., and S.X. wrote the draft manuscript. All authors commented on and revised the manuscript. **Competing interests:** The authors declare no competing interests. **Data and materials availability:** The lunar sample, designated CE6C0010YJFMFM004, was provided by CNSA under a materials transfer agreement (*43*). The sample is presently held at the Beijing SHRIMP (sensitive high-resolution ion micro probe) Center on a 1-year loan (with a possible extension for another year), after which it will be returned to CNSA. Readers may request Chang'e-6 samples from CNSA through a standard procedure (*43*). Our calculated bulk compositions are provided in table S1, and the measured U-Pb and Pb-Pb data are provided in table S2. The textural classification of Chang'e-6 basalt images are available in data S1, electron microprobe data in data S2 and S4, the Pb-Pb data for reference glasses in data S5, the trace elements data in data S6 and S7, the calculated melt composition data in data S3, the MATLAB code used for μ-value calculation in data S8, and the SHRIMP, electron microprobe, and laser ablation spot images in data S9 and S10. **License information:** Copyright © 2025 the authors, some rights reserved; exclusive licensee American Association for the Advancement of Science. No claim to original US government works. https://www.science.org/about/science-licenses-journal-article-reuse

SUPPLEMENTARY MATERIALS

science.org/doi/10.1126/science.adt3332
Materials and Methods
Supplementary Text
Figs. S1 to S6
Tables S1 and S2
References (*44*–*76*)
Data S1 to S10

Submitted 24 September 2024; accepted 13 February 2025
Published online 27 February 2025
10.1126/science.adt3332